A Photometric Study of the Contact Binary V384 Serpentis

Edward J. Michaels
Stephen F. Austin State University, Department of Physics, Engineering and Astronomy, P.O. Box 13044, Nacogdoches, TX 75962; emichaels@sfasu.edu

Chlöe M. Lanning
Stephen F. Austin State University, Department of Physics, Engineering and Astronomy, P.O. Box 13044, Nacogdoches, TX 75962; chloelanning@gmail.com

Skyler N. Self
Stephen F. Austin State University, Department of Physics, Engineering and Astronomy, P.O. Box 13044, Nacogdoches, TX 75962; skyler.self.23@gmail.com

Received January 20, 2019; revised March 26, 2019; accepted April 3, 2019

Abstract In this paper we present the first photometric light curves in the Sloan g', r', and i' passbands for the contact binary V384 Ser. Photometric solutions were obtained using the Wilson-Devinney program which revealed the star to be a W-type system with a mass ratio of q = 2.65 and a f = 36% degree of contact. The less massive component was found to be about 395 K hotter than the more massive one. A hot spot was modeled on the cooler star to fit the asymmetries of the light curves. By combining our new times of minima with those found in the literature, the (O–C) curve revealed a downward parabolic variation and a small cyclic oscillation with an amplitude of 0.0037 day and a period 2.86 yr. The downward parabolic change corresponds to a long-term decrease in the orbital period at a rate of $dP/dt = -3.6 \times 10^{-8}$ days yr^{-1}. The cyclic change was analyzed for the light-travel time effect that results from the gravitational influence of a close stellar companion.

1. Introduction

V384 Ser (GSC 02035-00175) was identified as an eclipsing binary star by Akerlof *et al.* (2000) using data acquired by The Robotic Optical Transient Search Experiment I (ROTSE-I). An automated variable star classification technique using the Northern Sky Variability Survey (NSVS) classified this star as a W UMa contact binary (Hoffman *et al.* 2009). The machined-learned ASAS Classification Catalog gives the same classification (Richards 2012). Using ROTSE-I sky patrol data, Gettel *et al.* (2006) found an orbital period of 0.268739 day, a maximum visual magnitude of 11.853, and an amplitude of variation of 0.475 magnitude. The parallax measured by the Gaia spacecraft (DR2) gives a distance of d = 211 pc (Bailer-Jones *et al.* 2018). Data Release 4 from the Large Sky Area Multi-Object Fiber Spectroscopic Telescope survey (LAMOST) gives a spectral type of K2 (Luo *et al.* 2015). A ROSAT (Röntgen Satellite) survey of contact binary stars confirmed x-ray emission from V384 Ser (Geske *et al.* 2006). Using the Wide-Angle Search for Planets (SuperWASP) archive, Lohr *et al.* (2015) found evidence for a sinusoidal period change, which suggests a third body may be in the V384 Ser system.

Presented in this paper is the first photometric study of V384 Ser. The photometric observations and data reduction methods are presented in section 2, with new times of minima and a period study in section 3. Light curve analysis using the Wilson-Devinney model is presented in section 4. A discussion of the results is given in section 5 with conclusions in section 6.

2. Observations

Multi-band photometric observations were acquired with a robotic 0.36-m Ritchey-Chrétien telescope located at the Waffelow Creek Observatory (http://obs.ejmj.net/index.php). A SBIG-STXL camera equipped with a cooled (–30°) KAF-6303E CCD was used for image acquisition. Images were obtained in the Sloan g', r', and i' passbands on 4 nights in June 2017. These images comprise the first data set (DS1). A second set of data (DS2) was acquired on 13 nights in April and May 2018 which includes 1,555 images in the g' passband, 1361 in r', and 1935 in i'. For DS2 the exposure times were 40 s for the g' and i' passbands and 25 s for the r' passband. The observation's average S/N for V384 Ser in the g', r', and i' passbands was 264, 327, and 291, respectively. Bias, dark, and flat frames were taken each night. Image calibration and ensemble differential aperture photometry of the light images were performed using MIRA software (Mirametrics 2015). Both data sets were processed using the comparison stars shown on the AAVSO Variable Star Plotter (VSP) finder chart (Figure 1). The standard magnitudes of the comparison and check stars were taken from the AAVSO Photometric All-Sky Survey and are listed in Table 1 (APASS; Henden *et al.* 2015). The instrumental magnitudes of V384 Ser were converted to standard magnitudes using these comparison stars. The Heliocentric Julian Date of each observation was converted to orbital phase (φ) using the following epoch and orbital period: T_o = 2458251.6910 and P = 0.26872914 d. The folded light curves for DS2 are shown in Figure 2. All light curves in this paper were plotted from orbital phase –0.6 to 0.6 with negative phase defined as φ – 1. The check star magnitudes were plotted and inspected each night with no significant variability noted. The standard deviation of the check star magnitudes from DS2 (all nights) was 8 mmag for the g' passband, 5 mmag for r', and 6 mmag for i'. The check star magnitudes for each passband are plotted in the

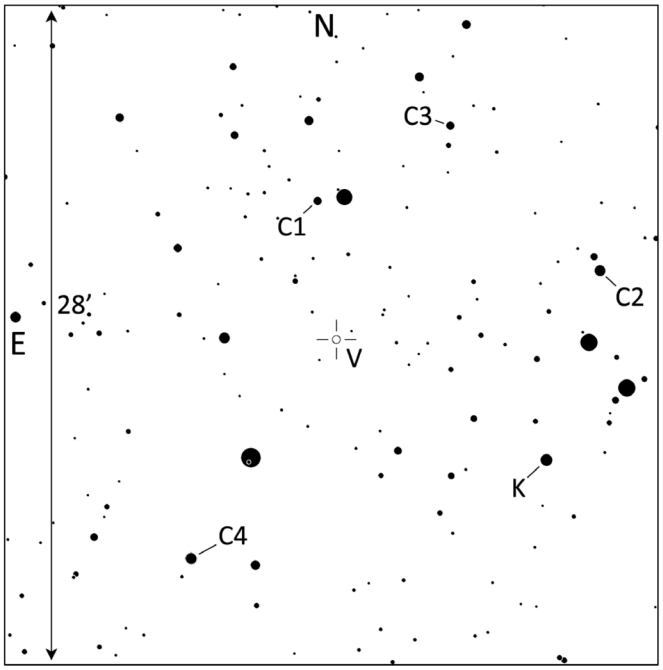

Figure 1. Finder chart for V384 Ser (V) showing the comparison (C1–C4) and check (K) stars.

Table 1. Stars used in this study.

Star	*R.A. (2000) h*	*Dec. (2000) °*	*g′*	*r′*	*i′*
V384 Ser	16.03154	+24.87153			
[1]GSC 02035-00369 (C1)	16.03254	+24.97094	13.400 ±0.230	12.679 ±0.074	12.394 ±0.087
[1]GSC 02035-00374 (C2)	16.01763	+24.92069	12.452 ±0.165	11.693 ±0.048	11.491 ±0.085
[1]GSC 02038-00840 (C3)	16.02552	+25.02490	13.085 ±0.227	12.659 ±0.086	12.534 ±0.105
[1]GSC 02035-00337 (C4)	16.03920	+24.71401	12.067 ±0.056	11.313 ±0.038	10.975 ±0.056
[2]GSC 02035-00035 (K)	16.02046	+24.78484	12.719 ±0.195	11.469 ±0.101	11.090 ±0.095
Means of observed K star magnitudes			12.490	11.474	11.083
Standard deviation of observed K star magnitudes			±0.008	±0.005	±0.006

APASS (Henden et al. *2015) [1]comparison stars (C1–C4) and [2]check star (K) magnitudes.*

bottom panel of Figure 2. New times of minimum light were determined from both the 2017 and 2018 data sets. The 2018 observations can be accessed from the AAVSO International Database (Kafka 2017).

3. Period study

Orbital period changes are an important observational property as well as an important component for understanding contact binaries. The orbital period changes of V384 Ser have not been investigated since its discovery. To study this property, we located 120 CCD eclipse timings in the literature. The minima times are listed in Table 2 along with 22 new eclipse timings from the observations in this study. This data set spans more than 18 years. The first primary minimum in Table 2 and

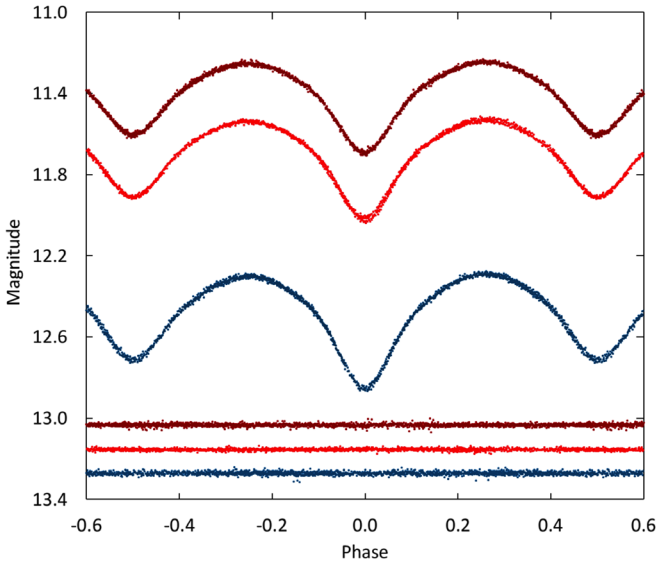

Figure 2. Folded light curves for each observed passband. The differential magnitudes of V384 Ser were converted to standard magnitudes using the calibrated magnitudes of the comparison stars. From top to bottom the light curve passbands are Sloan i', r' and g'. The bottom curves show the offset check star magnitudes in the same order as the light curves (offsets: i' = 1.95, r' = 1.68 and g' = 0.78). Error bars are not shown for clarity.

an orbital period taken from The International Variable Star Index (VSX) give the following linear ephemeris:

$$\text{HJD Min I} = 2451247.8121 + 0.268729 \times \text{E}. \quad (1)$$

This ephemeris was used to calculate the $(O–C)_1$ values in Table 2 with the corresponding $(O–C)_1$ diagram shown in the top panel of Figure 3 (black dots). A long-term decrease in the orbital period is apparent in the $(O–C)_1$ diagram (dashed line). In addition, a small amplitude cyclic variation is also clearly visible. We therefore combined a downward parabolic and a sinusoidal variation to describe the general trend of $(O–C)_1$ (solid line in Figure 3). By using the least-squares method, we derived

$$\begin{aligned}\text{HJD Min I} = {} & 2458251.6910(2) + 0.26872913(7) \times E \\ & -1.31(23) \times 10^{-11} \times E^2 \\ & + 0.0037(2) \sin(0.00162(1) \times E + 5.55\ (11)). \end{aligned} \quad (2)$$

The bottom panel of Figure 3 shows the residuals from Equation 2.

The quadratic term in Equation 2 gives the rate for the secular decrease in the orbital period, $dP/dt = –3.6(8) \times 10^{-8}$ days yr^{-1}, or 0.31 second per century. Subtraction of this continuous downward decrease gives the $(O–C)_2$ values shown in the middle panel of Figure 3. It displays the small amplitude periodic oscillation that overlaid the secular period decrease. The results of this period study will be discussed further in section 5.

4. Analysis

4.1. Temperature, spectral type

The temperature and spectral type of V384 Ser can be

Table 2. Times of minima and (O–C) residuals from Equation 1.

Epoch HJD 2400000+	*Error*	*Cycle*	$(O–C)_1$	*References*
51247.8121	0.0001	0.0	0.00000	Blättler and Diethelm 2002
51287.7189	0.0007	148.5	0.00054	Blättler and Diethelm 2002
52019.8715	0.0001	2873.0	0.00098	Nelson 2002
52038.8169	0.0001	2943.5	0.00099	Nelson 2002
52359.4103	0.0011	4136.5	0.00069	Blättler and Diethelm 2002
52360.4871	0.0007	4140.5	0.00258	Blättler and Diethelm 2002
52360.6191	0.0011	4141.0	0.00021	Blättler and Diethelm 2002
52365.4569	0.0008	4159.0	0.00089	Blättler and Diethelm 2002
52365.5911	0.0005	4159.5	0.00072	Blättler and Diethelm 2002
52368.4142	0.0018	4170.0	0.00217	Blättler and Diethelm 2002
52368.5471	0.0003	4170.5	0.00071	Blättler and Diethelm 2002
52395.4223	0.0017	4270.5	0.00301	Blättler and Diethelm 2002
52395.5540	0.0003	4271.0	0.00034	Blättler and Diethelm 2002
52409.3972	0.0007	4322.5	0.00400	Blättler and Diethelm 2002
52409.5282	0.0006	4323.0	0.00063	Blättler and Diethelm 2002
52415.5762	0.0002	4345.5	0.00223	Blättler and Diethelm 2002
52763.4509	0.0002	5640.0	0.00724	Diethelm 2003
53216.3884	0.0004	7325.5	0.00201	Diethelm 2005
53541.4207	0.0008	8535.0	0.00659	Diethelm 2005
53917.5096	0.0009	9934.5	0.00925	Diethelm 2006
54197.3869	0.0009	10976.0	0.00530	Diethelm 2007
54516.6359	0.0005	12164.0	0.00424	Hübscher, *et al.* 2009a
54570.3803	0.0003	12364.0	0.00284	Hübscher, *et al.* 2009b
54583.4154	0.0003	12412.5	0.00459	Hübscher, *et al.*2009b
54583.5492	0.0003	12413.0	0.00402	Hübscher, *et al.* 2009b
54594.4335	0.0002	12453.5	0.00480	Hübscher, *et al.* 2009a
54594.5664	0.0002	12454.0	0.00333	Hübscher, *et al.* 2009a
54596.4472	0.0002	12461.0	0.00303	Hübscher, *et al.* 2009a
54596.5811	0.0005	12461.5	0.00257	Hübscher, *et al.* 2009a
54597.3894	0.0002	12464.5	0.00468	Hübscher, *et al.* 2009a
54597.5232	0.0002	12465.0	0.00412	Hübscher, *et al.* 2009a
54604.1058	—	12489.5	0.00285	Kazuo 2009
54610.4225	0.0002	12513.0	0.00442	Hübscher, *et al.* 2009a
54610.5568	0.0004	12513.5	0.00436	Hübscher, *et al.* 2009a
54636.4897	0.0002	12610.0	0.00491	Hübscher, *et al.* 2009a
54684.4597	0.0006	12788.5	0.00678	Diethelm 2009a
54703.4042	0.0002	12859.0	0.00589	Hübscher, *et al.* 2009a
54934.3748	0.0003	13718.5	0.00391	Hübscher, *et al.* 2010
54934.5081	0.0001	13719.0	0.00285	Hübscher, *et al.* 2010
54943.3768	0.0008	13752.0	0.00349	Hübscher, *et al.* 2010
54943.5111	0.0006	13752.5	0.00343	Hübscher, *et al.* 2010
54959.4998	0.0003	13812.0	0.00275	Hübscher, *et al.* 2010
54961.6506	0.0005	13820.0	0.00372	Diethelm 2009b
54961.7836	0.0001	13820.5	0.00236	Diethelm 2009b
54961.9198	0.0010	13821.0	0.00419	Diethelm 2009b
54996.4497	0.0003	13949.5	0.00241	Hübscher, *et al.* 2010
55029.3681	0.0003	14072.0	0.00151	Hübscher, *et al.* 2010
55029.3688	0.0004	14072.0	0.00221	Diethelm 2010a
55029.5003	0.0003	14072.5	–0.00065	Hübscher, *et al.* 2010
55038.3694	0.0006	14105.5	0.00039	Diethelm 2010a
55038.5057	0.0004	14106.0	0.00233	Diethelm 2010a
55049.3857	0.0005	14146.5	–0.00120	Hübscher, *et al.* 2011
55269.8770	0.0001	14967.0	–0.00204	Diethelm 2010b
55293.3921	0.0081	15054.5	–0.00073	Hübscher, *et al.* 2011
55293.5257	0.0002	15055.0	–0.00150	Hübscher, *et al.* 2011
55304.4085	0.0002	15095.5	–0.00222	Hübscher, *et al.* 2011
55304.5437	0.0003	15096.0	–0.00138	Hübscher, *et al.* 2011
55309.5149	0.0002	15114.5	–0.00167	Hübscher, *et al.* 2011
55376.4290	0.0005	15363.5	–0.00109	Hübscher, *et al.* 2011
55397.5233	0.0004	15442.0	–0.00202	Hübscher, *et al.* 2011
55629.5769	0.0016	16305.5	0.00409	Hübscher, *et al.* 2012
55653.8944	0.0001	16396.0	0.00162	Diethelm 2011
55662.4937	0.0003	16428.0	0.00159	Hübscher and Lehmann 2012
55689.5043	0.0004	16528.5	0.00492	Hübscher and Lehmann 2012
55754.4014	0.0002	16770.0	0.00397	Hübscher and Lehmann 2012
55754.5363	0.0005	16770.5	0.00451	Hübscher and Lehmann 2012
55775.3623	0.0009	16848.0	0.00401	Hübscher and Lehmann 2012
56008.4824	0.0003	17715.5	0.00170	Hübscher, *et al.* 2013
56008.6162	0.0001	17716.0	0.00114	Hübscher, *et al.* 2013
56035.8890	0.0030	17817.5	–0.00206	Diethelm 2012
56045.4316	0.0002	17853.0	0.00066	Hübscher, *et al.* 2013
56045.5651	0.0001	17853.5	–0.00020	Hübscher, *et al.* 2013
56065.4508	0.0002	17927.5	–0.00045	Hübscher, *et al.* 2013
56080.3651	0.0001	17983.0	–0.00061	Gürsoytrak *et al.* 2013
56080.4991	0.0006	17983.5	–0.00097	Gürsoytrak *et al.* 2013
56087.3527	0.0003	18009.0	0.00004	Terzioğlu, *et al.* 2017
56087.4848	0.0008	18009.5	–0.00223	Terzioğlu, *et al.* 2017
56094.4726	0.0003	18035.5	–0.00138	Hübscher, *et al.* 2013
56132.3628	0.0011	18176.5	–0.00197	Hübscher, *et al.* 2013
56132.4991	0.0004	18177.0	–0.00003	Hübscher, *et al.* 2013
56407.4080	0.0006	19200.0	–0.00090	Hübscher 2013
56407.5396	0.0002	19200.5	–0.00366	Hübscher 2013
56475.3965	0.0004	19453.0	–0.00084	Hübscher 2013
56475.5292	0.0003	19453.5	–0.00250	Hübscher 2013
56505.3579	0.0015	19564.5	–0.00272	Hübscher 2014
56505.4949	0.0005	19565.0	–0.00009	Hübscher 2014
56834.4254	0.0008	20789.0	0.00612	Hübscher and Lehmann 2014
56856.4598	0.0004	20871.0	0.00474	Hübscher and Lehmann 2014
56864.3876	0.0003	20900.5	0.00504	Hoňková, *et al.* 2015
56924.3124	0.0030	21123.5	0.00327	Hübscher 2015
57066.6013	0.0001	21653.0	0.00016	Jurysek, *et al.* 2017
57122.3618	0.0003	21860.5	–0.00060	Hübscher 2016
57122.4959	0.0002	21861.0	–0.00087	Hübscher 2016
57132.4396	0.0022	21898.0	–0.00014	Hübscher 2017
57132.5732	0.0026	21898.5	–0.00091	Hübscher 2017
57133.5137	0.0001	21902.0	–0.00096	Hübscher 2016
57134.4542	0.0002	21905.5	–0.00101	Hübscher 2016
57134.5884	0.0001	21906.0	–0.00117	Hübscher 2016
57153.3994	0.0003	21976.0	–0.00120	Hübscher 2016
57153.5338	0.0004	21976.5	–0.00117	Hübscher 2016
57158.3709	0.0034	21994.5	–0.00119	Hübscher 2016
57158.5038	0.0036	21995.0	–0.00266	Hübscher 2016
57225.6858	0.0002	22245.0	–0.00291	Samolyk 2016
57238.4509	0.0002	22292.5	–0.00243	Hübscher 2016
57241.4065	0.0002	22303.5	–0.00285	Hübscher 2016
57266.3980	0.0004	22396.5	–0.00315	Hübscher 2017
57499.3842	0.0002	23263.5	–0.00499	Hübscher 2017
57499.5191	0.0002	23264.0	–0.00446	Hübscher 2017
57508.3868	0.0001	23297.0	–0.00481	Hübscher 2017
57508.5205	0.0001	23297.5	–0.00548	Hübscher 2017
57513.7615	0.0001	23317.0	–0.00469	Nelson 2017
57514.4331	0.0001	23319.5	–0.00492	Hübscher 2017
57514.4351	0.0038	23319.5	–0.00292	Hübscher 2017
57514.5660	0.0018	23320.0	–0.00638	Hübscher 2017
57514.5677	0.0001	23320.0	–0.00468	Hübscher 2017
57515.3725	0.0010	23323.0	–0.00607	Hübscher 2017
57515.3740	0.0001	23323.0	–0.00457	Hübscher 2017
57515.5092	0.0017	23323.5	–0.00373	Hübscher 2017
57516.4489	0.0001	23327.0	–0.00458	Hübscher 2017
57516.5825	0.0005	23327.5	–0.00535	Hübscher 2017
57517.3889	0.0002	23330.5	–0.00513	Hübscher 2017
57517.5243	0.0003	23331.0	–0.00410	Hübscher 2017
57921.6990	0.0002	24835.0	0.00222	this paper
57921.8317	0.0002	24835.5	0.00049	this paper
57924.7878	0.0001	24846.5	0.00062	this paper
57932.7168	0.0001	24876.0	0.00211	this paper
57933.6566	0.0002	24879.5	0.00129	this paper
58224.8184	0.0001	25963.0	–0.00476	this paper
58225.7596	0.0001	25966.5	–0.00407	this paper
58225.8931	0.0001	25967.0	–0.00494	this paper
58231.8050	0.0001	25989.0	–0.00512	this paper
58244.7038	0.0001	26037.0	–0.00527	this paper
58245.6448	0.0001	26040.5	–0.00482	this paper
58245.7788	0.0001	26041.0	–0.00519	this paper
58246.7199	0.0001	26044.5	–0.00464	this paper
58247.7942	0.0001	26048.5	–0.00526	this paper
58248.7347	0.0001	26052.0	–0.00531	this paper
58248.8698	0.0001	26052.5	–0.00462	this paper
58249.6764	0.0001	26055.5	–0.00415	this paper
58249.8096	0.0001	26056.0	–0.00532	this paper
58250.7509	0.0001	26059.5	–0.00457	this paper
58250.8845	0.0001	26060.0	–0.00537	this paper
58251.6908	0.0001	26063.0	–0.00523	this paper
58257.7379	0.0001	26085.5	–0.00453	this paper

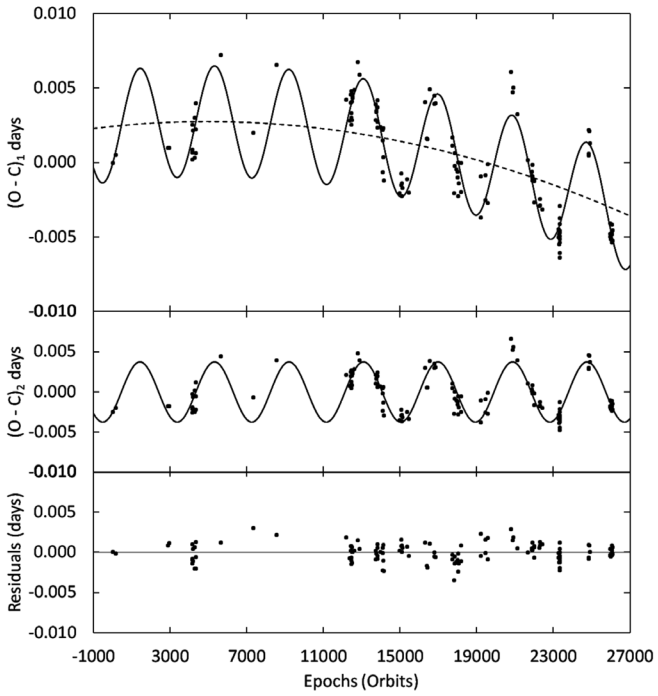

Figure 3. The top panel shows the $(O–C)_1$ diagram for all minimum times for V384 Ser. Black dots are residuals calculated from the linear ephemeris of Equation 1. The solid line corresponds to Equation 2 which is the combination of a long-term decrease and a small-amplitude cyclic variation. The dashed line refers to the quadratic term in this equation. In the middle panel the quadratic term of Equation 2 is subtracted to show the periodic variation more clearly. The bottom panel shows the residuals after removing the downward parabolic change and the cyclic variation.

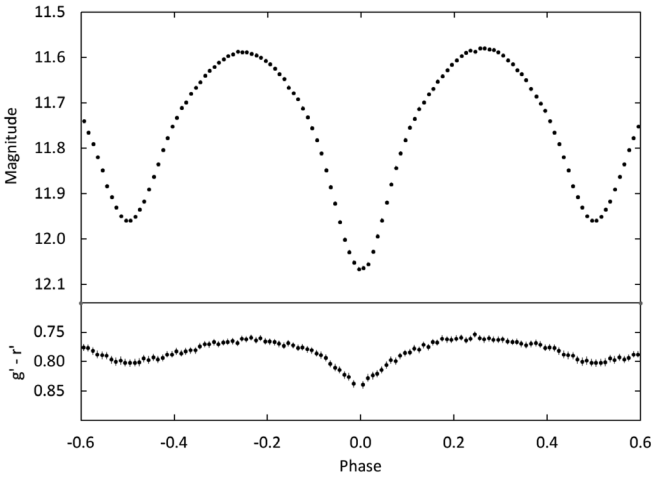

Figure 4. Light curve of all Sloan r'-band observations in standard magnitudes (top panel). The observations were binned with a phase width of 0.01. The errors for each binned point are about the size of the plotted points. The g'–r' colors were calculated by subtracting the linearly interpolated binned g' magnitudes from the linearly interpolated binned r' magnitudes.

measured from the star's color or its spectrum. The average (B–V) color index was determined from the DS2 observations. The phase and magnitude of the g' and r' observations were binned with a phase width of 0.01. The phases and magnitudes in each bin were averaged. The binned r' magnitudes were then subtracted from the linearly interpolated g' magnitudes. Figure 4 displays the binned r' magnitude light curve, with the bottom panel showing the (g'–r') color index. The average of the (g'–r') values over the entire phase range gives a color index of (g'–r') = 0.782 ±0.004. The (B–V) color was found using the Bilir *et al.* (2005) transformation equation,

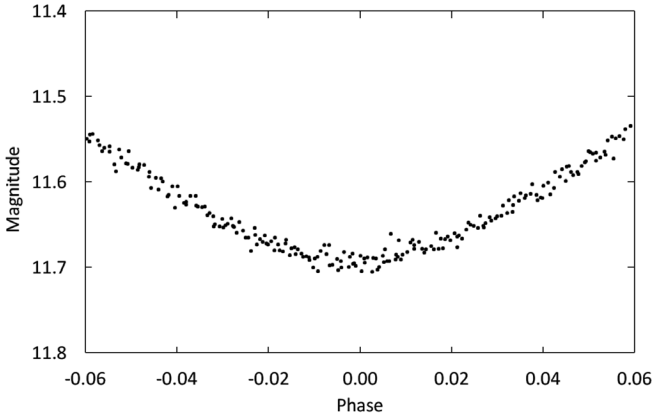

Figure 5. Observations of the primary eclipse portion of the Sloan r' light curve. Error bars are not shown for clarity.

$$(B–V) = \frac{(g'–r') + 0.25187}{1.12431} \quad . \qquad (3)$$

The average observed color of V384 Ser is (B–V) = 0.920 ± 0.003. This star's spectrum was acquired by the LAMOST telescope on April 19, 2014. The LAMOST DR4 catalog gives an effective temperature of T_{eff} = 4976 ± 18 K and a spectral class of K2. Using this temperature, the color was interpolated from the tables of Pecaut and Mamajek (2013), $(B–V)_o$ = 0.924 ± 0.009. This value agrees well with the observed photometric color, indicating the color excess for this star is very small. This result is not surprising, given the proximity of V384 Ser and its location well above the galactic equator (galactic latitude +47.4°).

4.2. Synthetic light curve modeling

The DS2 observations were used in the light curve analysis. The light curves showed only slight asymmetries and a small O'Connell effect with Max I (φ = 0.25) brighter than Max II (φ = 0.75) by only 0.009 magnitude in the g′ passband. Figure 5 shows a closeup of primary minimum, clearly showing the eclipse is not total. To decrease the total number of points used in modeling and to improve precision in the light curve solution, the observations were binned in both phase and magnitude with a phase interval of 0.01. On average, each binned data point was formed by 16 observations in the g' band, 14 in the r' band, and 19 in the i' band. For light curve modeling the binned magnitudes were converted to relative flux.

The BINARY MAKER 3.0 (BM3; Bradstreet and Steelman 2002) program was used to make the initial fit to each observed light curve using standard convective parameters and limb darkening coefficients from Van Hamm's (1993) tabular values. An initial mass ratio of q = 2.81 was computed using the period-mass relation for contact binaries,

$$\log M_1 = (0.352 \pm 0.166) \log P – (0.262 \pm 0.067), \qquad (4)$$
$$\log M_2 = (0.755 \pm 0.059) \log P + (0.416 \pm 0.024), \qquad (5)$$

where M_1 is the mass of the less massive star and P is the orbital period in days (Gazeas and Stępień 2008). In the BM3 analysis it was necessary to add a third light to fit the minima of the synthetic light curves to the observed light curves. The parameters resulting from the initial fits to each light curve were averaged. These averages were used as the initial input parameters for the computation of simultaneous three-color light curve solutions using the 2015 version of the Wilson-Devinney program (WD; Wilson and Devinney 1971; Van Hamme and Wilson 1998). The contact configuration (Mode 3) was set in the program since the observed light curves are typical of a short-period contact binary (W-type). Each binned input data point was assigned a weight equal to the number of observations forming that point. The temperature for the star eclipsed at primary minima was fixed at T_1 = 4976 K. The other fixed inputs include standard convective parameters: gravity darkening coefficients $g_1 = g_2 = 0.32$ (Lucy 1968) and bolometric albedos $A_1 = A_2 = 0.5$ (Ruciński 1969). Linear limb darkening coefficients were calculated by the program. The adjustable parameters include the orbital inclination (i), mass ratio ($q = M_2/M_1$), dimensionless surface potential (Ω, $\Omega_1 = \Omega_2$), temperature of star 2 (T_2), the normalized flux for each wavelength (L), and third light (ℓ).

The mass ratio (q) for V384 Ser is not known since there are no photometric or spectroscopic solutions available. Symmetrical light curves and total eclipses are very useful in determining reliable photometric solutions (Wilson 1978; Terrell and Wilson 2005). Since total eclipses are not seen in the light curves, we decided a mass ratio search (q-search) should be the first step in the solution process. A series of WD solutions were completed, each using a fixed mass ratio that ranged from 2.3 to 3.0 by steps of 0.02. The plot of the relation between the ΣResiduals^2 and the q values is shown in Figure 6. The minimum residual value was located at q = 2.65. This value was used as the starting mass ratio for the final solution iterations where the mass ratio was an adjustable parameter. The final best-fit solution is shown in column 2 of Table 3. The adjusted parameters are shown with errors, with the subscripts 1 and 2 referring to the primary and secondary stars eclipsed at Min I and Min II, respectively. The filling-factor in Table 3 was computed using the method of Lucy and Wilson (1979) given by

$$f = \frac{\Omega_{inner} - \Omega}{\Omega_{inner} - \Omega_{outer}} \quad , \qquad (6)$$

where Ω_{inner} and Ω_{outer} are the inner and outer critical equipotential surfaces and Ω is the equipotential that describes the stellar surface. Figure 7 shows the normalized light curves for each passband overlaid by the synthetic solution curves (solid lines) with the residuals shown in the bottom panel.

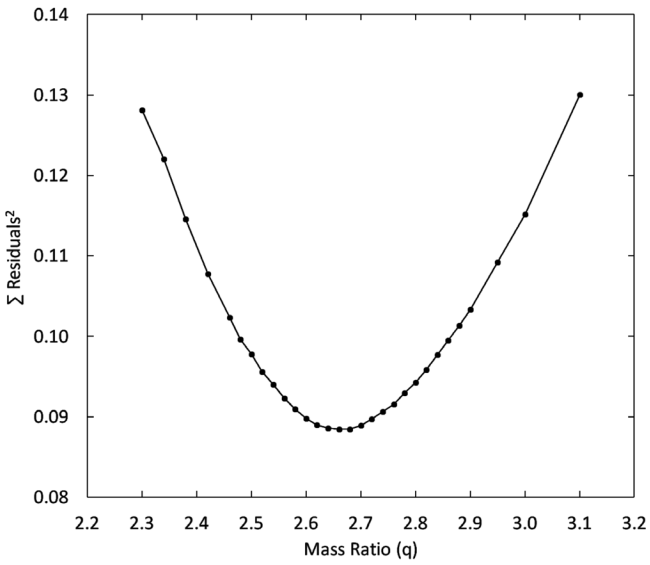

Figure 6. Results of the q-search showing the relation between the sum of the residuals squared and the mass ratio (q).

Table 3. Results derived from light curve modeling with spots.

Parameter	*Solution 1 (no spot)*	*Solution 1 (spot)*	*Solution 2 (spot)*
phase shift	–0.0009 ± 0.0002	0.0000 ± 0.0001	0.0000 ± 0.0001
filling factor	36%	36%	15%
i (°)	78.7 ± 1.1	78.6 ± 0.6	70.4 ± 0.6
T_1 (K)	[1]4976	[1]4976	[1]4976
T_2 (K)	4566 ± 7	4580 ± 5	4595 ± 4
$\Omega_1 = \Omega_2$	5.94 ± 0.09	5.94 ± 0.04	5.99 ± 0.02
$q(M_2/M_1)$	2.66 ± 0.06	2.65 ± 0.03	2.60 ± 0.01
$L_1/(L_1+L_2)$(g')	0.422 ± 0.007	0.417 ± 0.004	0.411 ± 0.010
$L_1/(L_1+L_2)$(r')	0.393 ± 0.007	0.390 ± 0.004	0.384 ± 0.009
$L_1/(L_1+L_2)$(i')	0.376 ± 0.007	0.373 ± 0.004	0.368 ± 0.009
ℓ_3 (g')	[2]0.24 ± 0.02	[2]0.24 ± 0.01	[2]0.02 ± 0.03
ℓ_3 (r')	[2]0.28 ± 0.02	[2]0.27 ± 0.01	[2]0.04 ± 0.03
ℓ_3 (i')	[2]0.29 ± 0.02	[2]0.29 ± 0.02	[2]0.07 ± 0.02
r_1 side	0.303 ± 0.003	0.305 ± 0.001	0.300 ± 0.001
r_2 side	0.510 ± 0.011	0.487 ± 0.005	0.470 ± 0.002
Σres^2	0.088	0.044	0.042
Spot Parameters		*Star 2—hot spot*	*Star 2—hot spot*
colatitude (°)		88 ± 7	92 ± 2
longitude (°)		12 ± 9	8 ± 5
spot radius (°)		10 ± 5	10 ± 4
temp.-factor		1.15 ± 0.05	1.15 ± 0.04

[1]*Assumed.*
[2]*Third lights are the percent of light contributed at orbital phase 0.25.*
The subscripts 1 and 2 refer to the star being eclipsed at primary and secondary minimum, respectively.
Note: The errors in the stellar parameters result from the least-squares fit to the model. The actual uncertainties of the parameters are considerably larger.

4.3. Spot model

The cool stars of contact binaries have a deep common convective envelope. Stars with this property produce a strong dynamo and display solar type magnetic activity. This activity manifests itself as cool regions (dark spots) or hot regions such as faculae in the star's photosphere. The O'Connell effect, where the light curves display unequal maxima, is usually attributed to spots on one or both stars. For V384 Ser, the DS2 light curves (Figure 2) show only a very weak O'Connell effect, but 11 months earlier the DS1 light curves had a pronounced O'Connell effect. This change can be seen in Figure 8, which shows the r' passband light curve for the 2017 observations (open circles) overlaid by the 2018 observations. Not only are season-to-season changes occurring in this star, but

night-to-night changes were also observed in the 2018 data. These observations confirm V384 Ser is magnetically active with changing spot configurations. It should also be noted that V384 Ser is an x-ray source, which is another key indication of magnetic activity (Geske *et al.* 2006).

The fit between the synthetic and observed light curves shows excess light between orbital phase 0.2 and 0.4 and a small light loss between 0.6 and 0.8 (see Figure 7). To fit these asymmetries, an over-luminous spot was modeled with BM3 in the neck region of the larger cooler star. The spot parameters, latitude, longitude, spot size, and temperature were adjusted until asymmetries were minimized. The resulting spot parameters were then incorporated into a new WD model. The spot model resulted in an improved fit between the observed and synthetic light curves, with a 50% reduction in the residuals compared to the spotless model. The final solution parameters for the spot model are shown in column 3 of Table 3. Figure 9 displays the model fit (solid lines) to the observed light curves and the residuals. Figure 10 shows a graphical representation of the spotted model that was created using BM3 (Bradstreet and Steelman 2002).

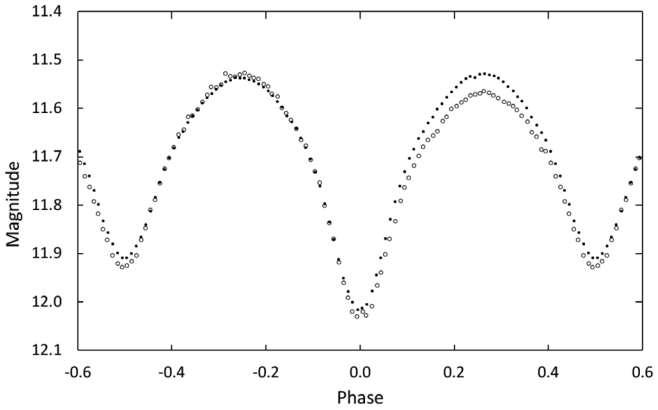

Figure 8. Comparison of 2017 and 2018 Sloan r' band light curves in standard magnitudes. The observations were binned with a phase width of 0.01. The 2017 observations (open circles) were acquired about 11 months before the 2018 observations (black dots).

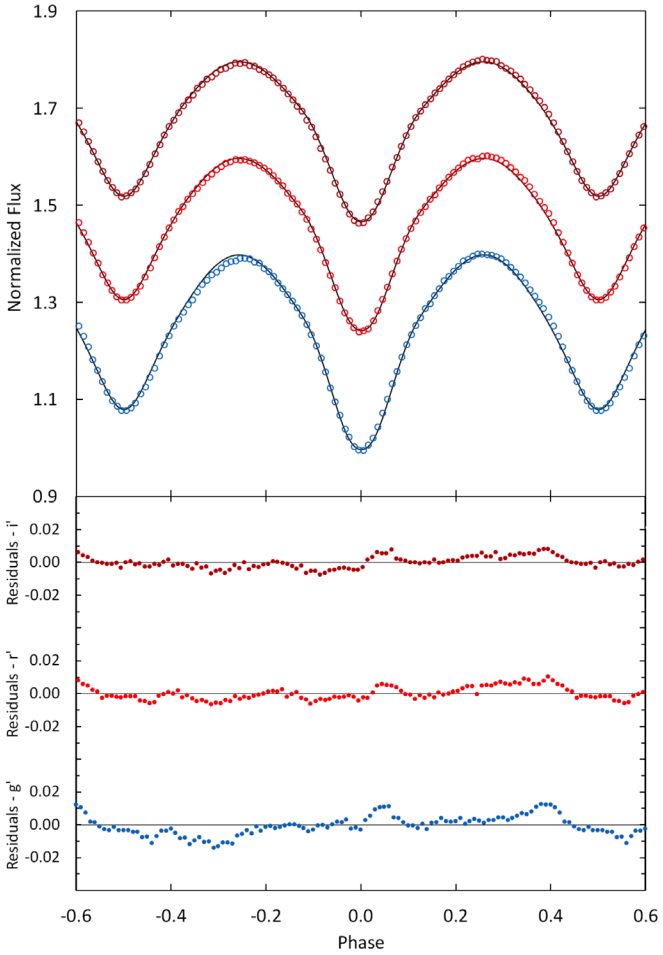

Figure 7. The observational light curves (open circles) and the fitted light curves (solid lines) for the spotless WD Solution 1 model (top panel). From top to bottom the passbands are Sloan i', r', and g' (each curve offset by 0.2). The residuals for the best-fit spotless model are shown in the bottom panel. Error bars are omitted from the points for clarity.

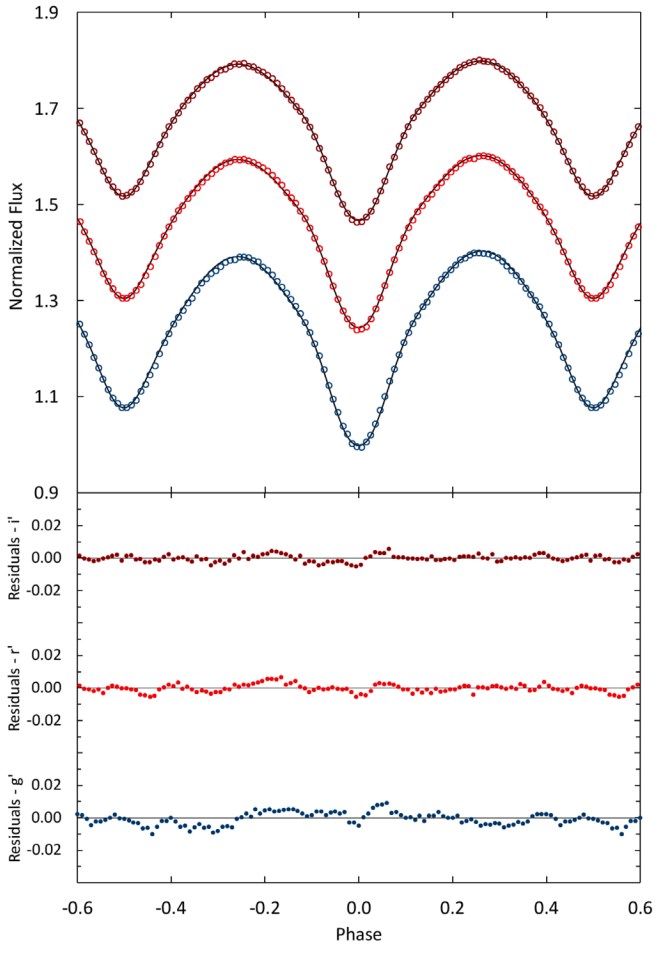

Figure 9. The observational light curves (open circles) and the fitted light curves (solid lines) for the spotted WD Solution 1 model (top panel). From top to bottom the passbands are Sloan i', r', and g' (each curve offset by 0.2). The residuals for the best-fit spot model are shown in the bottom panel. Error bars are omitted from the points for clarity.

5. Discussion

The absolute parameters of the component stars can be determined if their masses are known. Using the mass-period relation for contact binaries (Equation 5), the estimated mass of the larger cooler secondary star is $M_2 = 0.97 \pm 0.09\, M_\odot$ and a derived a primary mass gives $M_1 = 0.36 \pm 0.04\, M_\odot$. The distance between the mass centers, $1.93 \pm 0.05\, R_\odot$, was calculated using Kepler's Third Law. With this orbital separation, the WD light curve program (LC) calculated the stellar radii, luminosities, bolometric magnitudes, and surface gravities. The estimated absolute stellar parameters are collected in Table 4.

The luminosity of V384 Ser was calculated from the measured distance, the observed apparent V magnitude, and the bolometric correction (BCv). The Gaia parallax (DR2) gives a distance of d = 211 ± 2 pc (Bailer-Jones *et al.* 2018). The observed visual magnitude was determined from the DS2 observations using the average g' and r' passband values and the transformation equation of Jester *et al.* (2005),

$$V = g' - 0.59\,(g' - r') - 0.1. \qquad (7)$$

The resulting magnitude, V = 12.01 ± 0.04, agrees well with the APASS (DR9) value of V = 12.01 ± 0.19. As shown in section 4.1, the color excess for this star was very small, therefore, extinction was not applied to the V magnitude. The bolometric correction, $BC_v = -0.328$, was interpolated from the tables of Pecaut and Mamajek (2013) using the color from the LAMOST spectrum. The calculated absolute visual magnitude, visual luminosity, bolometric magnitude, and luminosity are given by $M_v = 5.38 \pm 0.8$, $L_v = 0.62 \pm 0.05\, L_\odot$, $M_{bol} = 5.06 \pm 0.08$, and $L = 0.75\, L_\odot \pm 0.05$, respectively. This luminosity is in good agreement with the value from Gaia DR2, $L = 0.71 \pm 0.01\, L_\odot$ (Gaia 2016, 2018).

The period study of section 3 found a short-term cyclic period change superimposed on a long-term secular decrease in the orbital period. A secular decreasing period could be explained by magnetic braking or by conservative mass exchange. For conservative mass exchange, transfer of matter from the larger more massive star to the smaller hotter companion would be required. For this case, the rate of mass transfer calculated from the well-known equation,

$$\frac{dM}{dt} = \frac{\dot{P} M_1 M_2}{3P(M_1 - M_2)}, \qquad (8)$$

gives a value of $7.09\ (0.01) \times 10^{-11}\, M_\odot$ / day (Reed 2011). The sinusoidally varying component of the ephemeris could be caused by magnetic activity (Applegate 1992) or the result of light-travel time effects caused by the orbital motion of the binary around a third body (Liao and Qian 2010; (Qian *et al.* 2013; Pribulla and Ruciński 2006). The modulation time of the orbital period due to magnetic activity can be estimated from the empirical relationship derived by Lanza and Rodonò (1999),

$$\log P_{mod} = -0.36(\pm 0.10) \log \Omega + 0.018, \qquad (9)$$

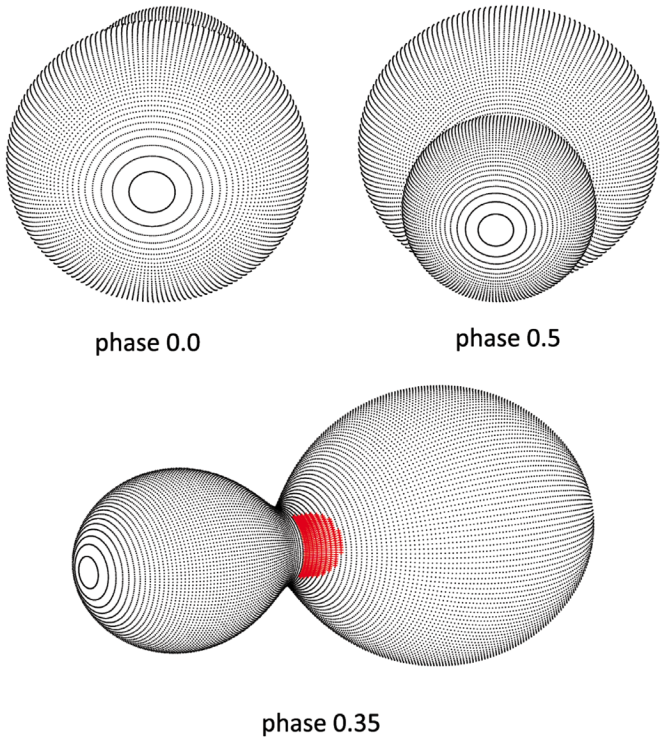

Figure 10. Roche Lobe surfaces of the best-fit WD spot model with orbital phase shown below each diagram.

Table 4. Estimated absolute parameters for V384 Ser.

Parameter	*Symbol*	*Value*
Stellar masses	$M_1\ (M_\odot)$	0.36 ± 0.04
	$M_2\ (M_\odot)$	0.97 ± 0.09
Semi-major axis	$a\ (R_\odot)$	1.93 ± 0.05
Mean stellar radii	$R_1\ (R_\odot)$	0.62 ± 0.01
	$R_2\ (R_\odot)$	0.94 ± 0.03
Stellar luminosity	$L_1\ (L_\odot)$	0.21 ± 0.01
	$L_2\ (L_\odot)$	0.35 ± 0.02
Bolometric magnitude	$M_{bol,1}$	6.43 ± 0.05
	$M_{bol,2}$	5.88 ± 0.07
Surface gravity	$\log g_1$ (cgs)	4.41 ± 0.04
	$\log g_2$ (cgs)	4.47 ± 0.04

Note: The calculated values in this table are provisional. Radial velocity observations are necessary for direct determination of M_1, M_2, and a.

where $\Omega = 2\pi / P$, P_{mod} is in years and P in seconds. Using the orbital period of V384 Ser gives a modulation period of about 20 years. This is about seven times longer than the observed modulation period, which makes magnetic activity an unlikely cause of the periodic variation. We analyzed the cyclic oscillation in the $(O-C)_2$ diagram (Figure 3, middle panel) for the light-travel time effect caused by a third stellar body orbiting V384 Ser. The sinusoidal term of Equation 2 gives the oscillation amplitude, $A_3 = 0.0037 \pm 0.0002$ days, and the third body's orbital period, $P_3 = 2.86 \pm 0.01$ yr. The orbit is likely circular, given the good sinusoidal fit over the several orbits covered by the observations. Assuming an orbital eccentricity of zero, the projected distance between the barycenter of the triple system and the binary was calculated from the equation:

$$a'_{12} \sin i' = A_3 \times c, \quad (10)$$

where i' is the orbital inclination of the third body and c is the speed of light. The mass function was determined from the following equation:

$$f(m) = \frac{4\pi^2}{GP_3^2} \times (a'_{12} \sin i')^3, \quad (11)$$

where G is the gravitational constant. By using the masses of the primary and secondary stars determined previously, the mass and orbital radius for the third stellar body were calculated from the following equation:

$$f(m) = \frac{(M_3 \sin i')}{(M_1 + M_2 + M_3)}. \quad (12)$$

For coplanar orbits (i' = 78.6°), the computed third body's mass and orbital radius are $M_3 = 0.49 \pm 0.03\ M_\odot$ and $a_3 = 1.80 \pm 0.05$ AU. The derived parameters are shown in Table 5, and the relation between the orbital inclination and the mass and orbital radius of the third body are shown in Figure 11. The properties of the third stellar body can now be approximated. Subtracting the luminosity for each binary component from the system luminosity gives a third body luminosity of $L_3 = 0.19 \pm 0.06\ L_\odot$. A main-sequence star of this luminosity has a color of (B–V) = 1.10, a temperature of T_{eff} = 4620 K, and a mass of 0.73 $M_\odot$ (Pecaut and Mamajek 2013). For comparison, the third star's color and temperature can be estimated from the third light values of Solution 1. Interpolating from the tables of Pecaut and Mamajek (2013) gives a color of (B–V) = 1.01 and a temperature of T_{eff} = 4800 K, which are reasonably close to the values found above. The estimated spectral type for the tertiary component is K3 or K4 with a mass between 0.7 – 0.8 $M_\odot$. For the estimated mass, the orbital inclination (i') of the third body would be about 45° (see Table 5 and Figure 11).

Close binaries in triple systems have resulted in spurious photometric solutions and V384 Ser is a good example (Gazeas and Niarchos 2006). The light curve analysis for this star resulted in a second WD solution that is shown in column 4 of Table 3 (Solution 2). The fit between the synthetic and observed light curves for Solution 2 are nearly identical to Solution 1. The residuals for Solution 2 are slightly smaller than Solution 1. The parameter sets differed primarily in orbital inclination, third light, and the filling factor, which are two very different solutions. To determine the best solution, we compared the observed total system luminosity to the luminosity of the binary. For Solution 1, the luminosity of the binary is $L_{12} = 0.56 \pm 0.03\ L_\odot$. The binary contributes about 74% of the total system light with the remaining 26% coming from a third source. This is a close match to the third lights found in Solution 1 (24%–29%). For Solution 2, the binary contributes 70% to the total system light with 30% coming from a third source. The third lights from Solution 2 are much smaller (2%–7%). The results from this analysis, plus the observed near total primary eclipse, supports Solution 1 with its higher orbital inclination.

Table 5. Parameters of the tertiary component.

Parameter	*Value*	*Units*
P_3	2.86 ± 0.01	years
A_3	0.0037 ± 0.0002	days
e'	0.0	assumed
$a'_{12} \sin i'$	0.65 ± 0.03	AU
f(m)	0.033 ± 0.005	$M_\odot$
M_3 (i' = 90°)	0.47 ± 0.03	$M_\odot$
M_3 (i' = 80°)	0.48 ± 0.03	$M_\odot$
M_3 (i' = 70°)	0.51 ± 0.03	$M_\odot$
M_3 (i' = 60°)	0.57 ± 0.03	$M_\odot$
M_3 (i' = 50°)	0.66 ± 0.04	$M_\odot$
M_3 (i' = 40°)	0.83 ± 0.05	$M_\odot$
a_3 (i' = 90°)	1.80 ± 0.05	AU
a_3 (i' = 80°)	1.80 ± 0.05	AU
a_3 (i' = 70°)	1.78 ± 0.05	AU
a_3 (i' = 60°)	1.75 ± 0.05	AU
a_3 (i' = 50°)	1.69 ± 0.05	AU
a_3 (i' = 40°)	1.60 ± 0.06	AU

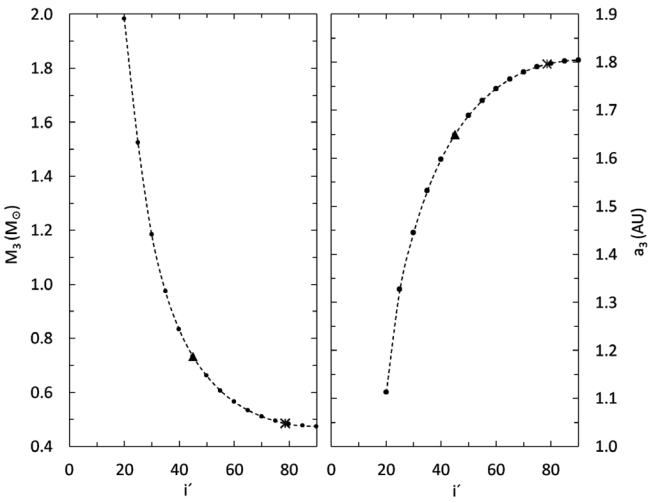

Figure 11. The relation between the third body's mass M_3 and the orbital inclination is shown in the left panel. The right panel shows the relation between the orbital radius and orbital inclination for the third body. The asterisk gives the mass and orbital radius for the tertiary component that is coplanar with V384 Ser and the solid triangle locates the orbital inclination (45°) for the estimated mass of the tertiary component.

6. Conclusions

This paper presents and analyzes the first complete set of photometric CCD observations in the Sloan g', r', and i' passbands for the eclipsing binary V384 Ser. This study confirms it is a W-type contact binary, where the larger more massive star is cooler and has less surface brightness than its companion. The best-fit WD solution gives a mass ratio of q = 2.65, a fill-out of f = 36%, and a temperature difference of 376 K between the component stars. This star was found to be magnetically active, as evidenced by changes in the light curves between observing seasons. The period analysis revealed V384 Ser is a triple system with a cool stellar companion having an orbital radius of about 1.7 AU. Early dynamical interaction between the stars may have had a significant influence in the evolution of this system. A spectroscopic study would be invaluable in confirming the stellar masses and mass ratio found

in the photometric solution presented here. In addition, the third stellar body may also have sufficient luminosity to be detected by high resolution spectroscopy.

7. Acknowledgements

This research was made possible through the use of the AAVSO Photometric All-Sky Survey (APASS), funded by the Robert Martin Ayers Sciences Fund. This research has made use of the SIMBAD database and the VizieR catalogue databases (operated at CDS, Strasbourg, France). This work has made use of data from the European Space Agency (ESA) mission Gaia (https://www.cosmos.esa.int/gaia), processed by the Gaia Data Processing and Analysis Consortium (DPAC, https://www.cosmos.esa.int/web/gaia/dpac/consortium). Funding for the DPAC has been provided by national institutions, in particular the institutions participating in the Gaia Multilateral Agreement. Data from the Guo Shou Jing Telescope (the Large Sky Area Multi-Object Fiber Spectroscopic Telescope, LAMOST) was also used in this study. This telescope is a National Major Scientific Project built by the Chinese Academy of Sciences. Funding for the project has been provided by the National Development and Reform Commission. LAMOST is operated and managed by National Astronomical Observatories, Chinese Academy of Sciences.

References

Akerlof, C., *et al.* 2000, *Astron. J.*, **119**, 1901.
Applegate, J. H. 1992, *Astrophys. J.*, **385**, 621.
Bailer-Jones, C., Rybizki, J., Fouesneau, M., Mantelet, G., and Andrae, R. 2018, *Astron. J.*, **156**, 58.
Bilir, S., Karaali, S., and Tunçel, S. 2005, *Astron. Nachr.*, **326**, 321.
Blättler, E., and Diethelm, R. 2002, *Inf. Bull. Var. Stars*, No. 5295, 1.
Bradstreet, D. H., and Steelman, D. P. 2002, *Bull. Amer. Astron. Soc.*, **34**, 1224.
Diethelm, R. 2003, *Inf. Bull. Var. Stars*, No. 5438, 1.
Diethelm, R. 2005, *Inf. Bull. Var. Stars*, No. 5653, 1.
Diethelm, R. 2006, *Inf. Bull. Var. Stars*, No. 5713, 1.
Diethelm, R. 2007, *Inf. Bull. Var. Stars*, No. 5781, 1.
Diethelm, R. 2009a, *Inf. Bull. Var. Stars*, No. 5871, 1.
Diethelm, R. 2009b, *Inf. Bull. Var. Stars*, No. 5894, 1.
Diethelm, R. 2010a, *Inf. Bull. Var. Stars*, No. 5920, 1.
Diethelm, R. 2010b, *Inf. Bull. Var. Stars*, No. 5945, 1.
Diethelm, R. 2011, *Inf. Bull. Var. Stars*, No. 5992, 1.
Diethelm, R. 2012, *Inf. Bull. Var. Stars*, No. 6029, 1.
Gaia Collaboration, *et al.* 2016, *Astron. Astrophys.*, **595A**, 1.
Gaia Collaboration, *et al.* 2018, *Astron. Astrophys.*, **616A**, 1.
Gazeas, K., and Niarchos, P. G., 2006, *Mon. Not. Roy. Astron. Soc.*, **370**, L29.
Gazeas, K., and Stępień, K. 2008, *Mon. Not. Roy. Astron. Soc.*, **390**, 1577.
Geske, M., Gettel, S., and McKay, T. 2006, *Astron. J.*, **131**, 633.
Gettel, S. J., Geske, M. T., and McKay, T. A. 2006, *Astron. J.*, **131**, 621.
Gürsoytrak, H., *et al.* 2013, *Inf. Bull. Var. Stars*, No. 6075, 1.
Henden, A. A., *et al.* 2015, AAVSO Photometric All-Sky Survey, data release 9, (http:www.aavso.org/apass).
Hoffman, D. I., Harrison, T. E., and McNamara, B. J. 2009, *Astron. J.*, **138**, 466.
Hoňková, K., *et al.* 2015, *Open Eur. J. Var. Stars*, **168**, 1.
Hübscher, J. 2013, *Inf. Bull. Var. Stars*, No. 6084, 1.
Hübscher, J. 2014, *Inf. Bull. Var. Stars*, No. 6118, 1.
Hübscher, J. 2015, *Inf. Bull. Var. Stars*, No. 6152, 1.
Hübscher, J. 2016, *Inf. Bull. Var. Stars*, No. 6157, 1.
Hübscher, J. 2017, *Inf. Bull. Var. Stars*, No. 6196, 1.
Hübscher, J., Braune, W., and Lehmann, P. B. 2013, *Inf. Bull. Var. Stars*, No. 6048, 1.
Hübscher, J., and Lehmann, P. B. 2012, *Inf. Bull. Var. Stars*, No. 6026, 1.
Hübscher, J., and Lehmann, P. B. 2014, *Inf. Bull. Var. Stars*, No. 6149, 1.
Hübscher, J., Lehmann, P. B., Monninger, G., Steinbach, H.-M., and Walter, F. 2010, *Inf. Bull. Var. Stars*, No. 5918, 1.
Hübscher, J., Lehmann, P. B., and Walter, F. 2012, *Inf. Bull. Var. Stars*, No. 6010, 1.
Hübscher, J., and Monninger, G. 2011, *Inf. Bull. Var. Stars*, No. 5959, 1.
Hübscher, J., Steinbach, H.-M., and Walter, F. 2009a, *Inf. Bull. Var. Stars*, No. 5889, 1.
Hübscher, J., Steinbach, H.-M., and Walter, F. 2009b, *Inf. Bull. Var. Stars*, No. 5874, 1.
Juryšek, J., *et al.* 2017, *Open Eur. J. Var. Stars*, No. 179, 1.
Kafka, S. 2017, variable star observations from the AAVSO International Database (https://www.aavso.org/aavso-international-database).
Kazuo, N. 2009, *Bull. Var. Star Obs. League Japan*, No. 48, 1.
Lanza, A. F., and Rodonò, M. 1999, *Astron. Astrophys.*, **349**, 887.
Liao, W.-P., and Qian, S.-B. 2010, *Mon. Not. R. Astron. Soc.*, **405**, 1930.
Lohr, M. E., Norton, A. J., Payne, S. G., West, R. G., and Wheatley, P. J. 2015, *Astron. Astrophys.*, **578A**, 136.
Lucy, L. B. 1968, *Astrophys, J.*, **151**, 1123.
Lucy, L. B., and Wilson, R. E. 1979, *Astrophys, J.*, **231**, 502.
Luo, A.-Li, *et al.*, 2015, Res. *Astron. Astrophys.*, **15**, 1095.
Mirametrics. 2015, Image Processing, Visualization, Data Analysis, (http://www.mirametrics.com).
Nelson, R. H. 2002, *Inf. Bull. Var. Stars*, No. 5224, 1.
Nelson, R. H. 2017, *Inf. Bull. Var. Stars*, No. 6195, 1.
Pecaut, M. J., and Mamajek, E. E. 2013, *Astrophys. J., Suppl. Ser.*, 208, 9, (http://www.pas.rochester.edu/~emamajek/EEM_dwarf_UBVIJHK_colors_Teff.txt).
Pribulla, T., and Rucinski, S. M. 2006, *Astron. J.*, **131**, 2986.
Qian, S.-B., Liu, N.-P., Liao, W.-P., He, J.-J., Liu, L., Zhu, L.-Y., Wang, J.-J., and Zhao, E.-G. 2013, *Astron. J.*, **146**, 38.
Reed, P. A. 2011, in *Mass Transfer Between Stars: Photometric Studies, Mass Transfer—Advanced Aspects*, ed. H. Nakajima, InTech DOI: 10.5772/19744 (https://www.intechopen.com/books/mass-transfer-advanced-aspects/mass-transfer-between-stars-photometric-studies), 3.
Richards, J. W., Starr, D. L., Miller, A. A., Bloom, J. S., Butler, N. R., Brink, H., and Crellin-Quick, A. 2012, *Astrophys. J., Suppl. Ser.*, **203**, 32.

Ruciński, S. M. 1969, *Acta Astron.*, **19**, 245.
Samolyk, G. 2016, *J. Amer. Assoc. Var. Star Obs.*, **44**, 164.
Terrell, D., and Wilson, R. E. 2005, *Astrophys. Space Sci.*, **296**, 221.
Terzioğlu, Z., *et al.* 2017, *Inf. Bull. Var. Stars*, No. 6128, 1.
van Hamme, W. 1993, *Astron. J.*, **106**, 2096.
van Hamme, W., and Wilson, R. E. 1998, *Bull. Amer. Astron. Soc.*, **30**, 1402.
Wilson, R. E. 1978, *Astrophys. J.*, **224**, 885.
Wilson, R. E., and Devinney, E. J. 1971, *Astrophys. J.*, **166**, 605.